



Band symmetries and singularities in twisted multilayer graphene

E. J. Mele*

Department of Physics and Astronomy, University of Pennsylvania, Philadelphia, Pennsylvania 19104, USA

(Received 12 October 2011; revised manuscript received 9 December 2011; published 27 December 2011)

The electronic spectra of rotationally faulted graphene bilayers are calculated using a continuum formulation for small fault angles that identifies two distinct electronic states of the coupled system. The low-energy spectra of one state features a Fermi velocity reduction, which ultimately leads to pairwise annihilation and regeneration of its low-energy Dirac nodes. The physics in the complementary state is controlled by pseudospin selection rules that prevent a Fermi velocity renormalization and produce second generation symmetry-protected Dirac singularities in the spectrum. These results are compared with previous theoretical analyses and with experimental data.

DOI: [10.1103/PhysRevB.84.235439](https://doi.org/10.1103/PhysRevB.84.235439)

PACS number(s): 73.22.Pr, 77.55.Px, 73.20.-r

I. INTRODUCTION

The variation of the electronic properties of few-layer graphenes (FLGs) with their layer stacking is receiving increasing attention. FLGs represent a family of materials that bridge the pseudorelativistic properties of single-layer graphene with the more conventional semimetallic behavior of bulk graphite. The atomic registry of neighboring layers and stacking sequence are structural parameters that determine their electronic properties.¹⁻⁵ In twisted FLGs where the crystallographic axes of neighboring layers are misaligned by a rotation angle $\theta \neq n\pi/3$, the interlayer interactions produce remarkably rich physics that is being actively studied.⁶⁻²²

This paper presents a continuum theory of the low-energy electronic physics in twisted bilayer graphenes for small rotation angles, as illustrated in Fig. 1. Our approach reveals the existence of two distinct electronic states in this system that present quite different electronic properties. The behavior of one state is identified with the situation described by a frequently adopted continuum formulation of this problem.^{8,16} the interlayer coupling renormalizes the Fermi velocities of the individual layers and hybridizes their Dirac cones in the spectral region where they merge. In the complementary state, we find that the Fermi velocity renormalization is nearly completely prevented by a pseudospin selection rule and the interlayer hybridization inherits a novel momentum space geometry producing a set of second generation Dirac singularities. The behavior in this latter family agrees well with properties experimentally observed for rotationally faulted FLGs thermally grown on SiC (000 $\bar{1}$),^{9,11,15} suggesting that this physics is realized in this form of FLG. We briefly discuss the relation of our new results to prior theoretical and to experimental studies of these systems.

The physics described below is identified by consideration of the effects of the lattice symmetry on the low-energy electronic spectra. We show that the geometrical structure of the low spectrum is determined by a symmetry-allowed threefold anisotropy in the interlayer coupling amplitudes which, though absent from conventional two-center tight-binding models, occur in empirical models of interlayer coupling in graphite. We find that the sign of this anisotropy distinguishes two quite different electronic states of this system.

II. SPATIALLY MODULATED HOPPING

The coupling between the two sublattices in the two layers can be represented by a (position-dependent) 2×2 matrix operator $\hat{T}_{12}(\vec{r})$. As shown in Fig. 2, for small angle faults the registry between layers in the unit cell evolves smoothly from regions locally characterized by AB (region α), BA (β), and AA (γ). The smoothest possible supercell-periodic matrix-valued expression for $\hat{T}(\vec{r})$ is given by the expansion

$$\hat{T}_{12}(\vec{r}) = \hat{t}_0 + \sum_{n=1}^6 e^{i\vec{G}_n \cdot \vec{r}} \hat{t}_n, \quad (1)$$

with constant matrix coefficients \hat{t}_n and where \vec{G}_n are the six elements of the first star of reciprocal lattice vectors dual to the superlattice translations \vec{T}_1 and \vec{T}_2 . The matrix coefficients \hat{t}_n ($n = 1, 6$) can be determined from the couplings in the locally registered regions; for example, in the geometry of Fig. 2 the even elements of the first star have coefficients

$$\hat{t}_{n \text{ even}} = t_G \begin{pmatrix} e^{-i\vec{G}_n \cdot \vec{r}_\gamma} & e^{-i\vec{G}_n \cdot \vec{r}_\alpha} \\ e^{-i\vec{G}_n \cdot \vec{r}_\beta} & e^{-i\vec{G}_n \cdot \vec{r}_\gamma} \end{pmatrix} = t_G \begin{pmatrix} z & 1 \\ z^* & z \end{pmatrix}, \quad (2)$$

where $z = e^{2\pi i/3}$ and the coefficients for the odd elements are $t_{n \text{ odd}} = t_{n \text{ even}}^*$. The constant matrix has the form

$$\hat{t}_0 = \begin{pmatrix} c_{aa} & c_{ab} \\ c_{ba} & c_{bb} \end{pmatrix}, \quad (3)$$

with real coefficients satisfying $c_{aa} = c_{bb}$ and $c_{ab} = c_{ba}$. The interlayer operator of Eqs. (2) and (3) is thus parametrized by three real constants t_G , c_{aa} , and c_{ab} . We choose these coefficients so that the interlayer matrix $\hat{T}(\vec{r}_\alpha)$ matches the Slonczewski-Weiss-McClure (SWMcC) interlayer parameters γ_1 , γ_3 , and γ_4 for Bernal stacked graphite shown in the inset of Fig. 2,²⁴ with the results in Table I. We note that the γ_3 parameter (hopping between unaligned sublattices in the two layers) is comparable to γ_1 and that the γ_4 parameter (hopping between aligned and unaligned sublattice sites) is relatively weak.

The conventional continuum description of twisted bilayer graphene^{8,16} can be derived from the constant matrix \hat{t}_0 . The low-energy Hamiltonian is a long-wavelength expansion around the zone corner points in each layer; in this Dirac basis, the matrix elements in Eq. (1) acquire the phases

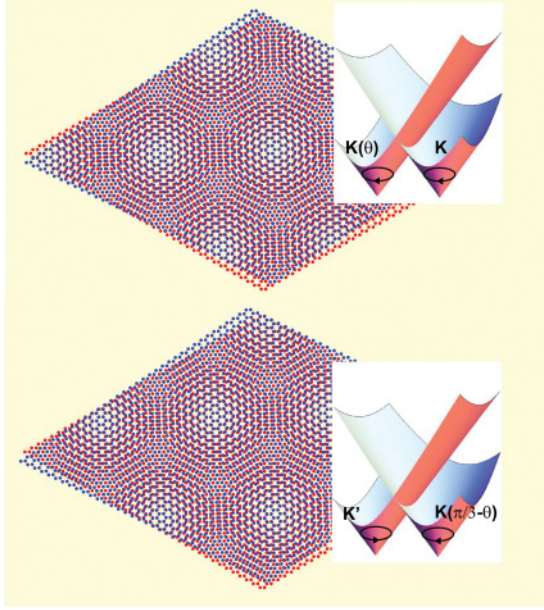


FIG. 1. (Color online) Lattice structures of twisted graphene bilayers rotated away from AA stacking by angles $\theta = 3.89^\circ$ (top) and its commensuration partner¹⁴ with $\theta = 56.11^\circ$ (bottom). The insets show schematically the dispersions of two nearby Dirac cones in these structures in the absence of their interlayer coupling.

$\exp[i(\vec{G}' \cdot \vec{\tau}'_i - \vec{G} \cdot \vec{\tau}_j)]$, where $\vec{G}(\vec{G}')$ are reciprocal lattice vectors in the two separate layers and $\vec{\tau}_j(\vec{\tau}'_i)$ are sublattice positions. Boosts by a triad of (\vec{G}, \vec{G}') pairs translate the Hamiltonian to three pairs of zone corner points that are separated by $\Delta\vec{K}$ and its $\pm 2\pi/3$ -rotated counterparts. This generates three possible constant coupling matrices indexed by the momentum differences $\Delta\vec{K}_i$. With a conventional choice of origin,^{8,16} where the A sublattice site of one layer is aligned

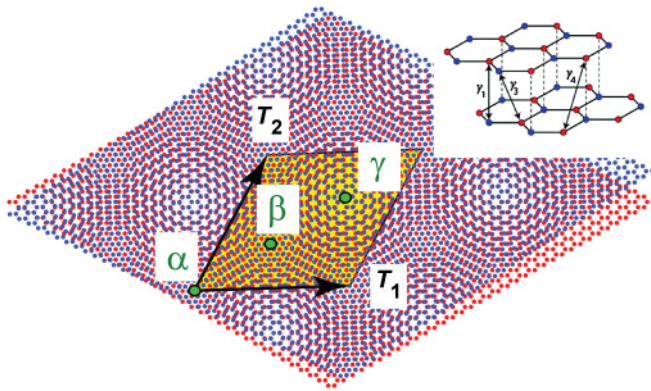


FIG. 2. (Color online) Lattice structure for a segment of twisted bilayer at rotation angle 3.89° , with superlattice translation vectors T_1 and T_2 . The points labeled α , β , and γ are high symmetry points in the unit cell. The inset²³ illustrates three hopping processes in the interlayer Hamiltonian.

TABLE I. Fourier coefficients (meV units) for the interlayer hopping operator Eq. (2), fitted to the Slonczewski-Weiss-McClure parametrization for Bernal stacked layers. Model I: $\gamma_1 = 390$ meV; $\gamma_3 = \gamma_4 = 0$. Model II: $\gamma_1 = 390$ meV, $\gamma_3 = 315$ meV, and $\gamma_4 = 44$ meV.

Coefficient	Parametrization	I	II
t_G	$(\gamma_1 - \gamma_3)/9$	43.3	8.3
c_{aa}	$\gamma_4 + (\gamma_1 - \gamma_3)/3$	130.0	69.0
c_{ab}	$(\gamma_1 + 2\gamma_3)/3$	130.0	340.0

with the B sublattice of the other, the matrices are

$$\begin{aligned} \hat{T}_1 &= \begin{pmatrix} 1 & 0 \\ 0 & 1 \end{pmatrix} \hat{t}_0 \begin{pmatrix} 1 & 0 \\ 0 & 1 \end{pmatrix} = \begin{pmatrix} c_{aa} & c_{ab} \\ c_{ba} & c_{bb} \end{pmatrix}, \\ \hat{T}_2 &= \begin{pmatrix} 1 & 0 \\ 0 & z \end{pmatrix} \hat{t}_0 \begin{pmatrix} z & 0 \\ 0 & 1 \end{pmatrix} = \begin{pmatrix} zc_{aa} & c_{ab} \\ z^*c_{ba} & zc_{bb} \end{pmatrix}, \\ \hat{T}_3 &= \begin{pmatrix} 1 & 0 \\ 0 & z^* \end{pmatrix} \hat{t}_0 \begin{pmatrix} z^* & 0 \\ 0 & 1 \end{pmatrix} = \begin{pmatrix} z^*c_{aa} & c_{ab} \\ zc_{ba} & z^*c_{bb} \end{pmatrix}. \end{aligned} \quad (4)$$

In one of these valleys, the Hamiltonian for the coupled bilayer with a momentum offset $\Delta\vec{K}$ is

$$H = \begin{pmatrix} \hbar v_F \sigma \cdot (-i\nabla) & \hat{T}_1^\dagger \\ \hat{T}_1 & \hbar v_F \sigma_\theta \cdot (-i\nabla - \Delta\vec{K}) \end{pmatrix}, \quad (5)$$

where σ_θ are Pauli matrices resolved along the axes of the θ -rotated layer. The problem can be written in dimensionless form by scaling all momenta by the offset $|\Delta\vec{K}|$ and energies by $E_\theta = \hbar v_F |\Delta\vec{K}|$. The scaled coupling coefficients are $\tilde{c} = c/E_\theta = 3ac/[8\pi\hbar v_F \sin(\theta/2)]$ (where a is the single-layer graphene lattice constant), which increase with decreasing rotation angle.

III. PARAMETRIZATIONS

Model I (Table I) is an isotropic interlayer model with $\gamma_3 = \gamma_4 = 0$. For an isotropic coupling model $c_{aa} = c_{bb} = w$ and the interlayer matrices are

$$\begin{aligned} \hat{T}_1 &= w \begin{pmatrix} 1 & 1 \\ 1 & 1 \end{pmatrix}, \quad \hat{T}_2 = w \begin{pmatrix} z & 1 \\ z^* & z \end{pmatrix}, \\ \hat{T}_3 &= w \begin{pmatrix} z^* & 1 \\ z & z^* \end{pmatrix}, \end{aligned} \quad (6)$$

with $w = 130$ meV. The form of these matrices and their prefactor agree with the estimates ($w \approx 110$ meV) obtained from tight-binding calculations.^{8,16} Our construction shows that these terms project the $q = 0$ term of the interlayer potential into the Dirac K -point (pseudospin) basis, thereby coupling the electronic states in the two layers with identical crystal momenta. Since only the $q = 0$ term in the coupling is retained, it does not depend on a relative lateral translation of the two layers, in agreement with earlier work¹⁶ and physically reasonable, since for small twist angle a rigid-layer translation produces insignificant changes to the Moiré superlattice. Thus model I reproduces the existing continuum theoretic phenomenology of the coupled system, and the calculation leading to Eq. (6) provides an alternate (and compact) derivation of the effective Hamiltonian used in these

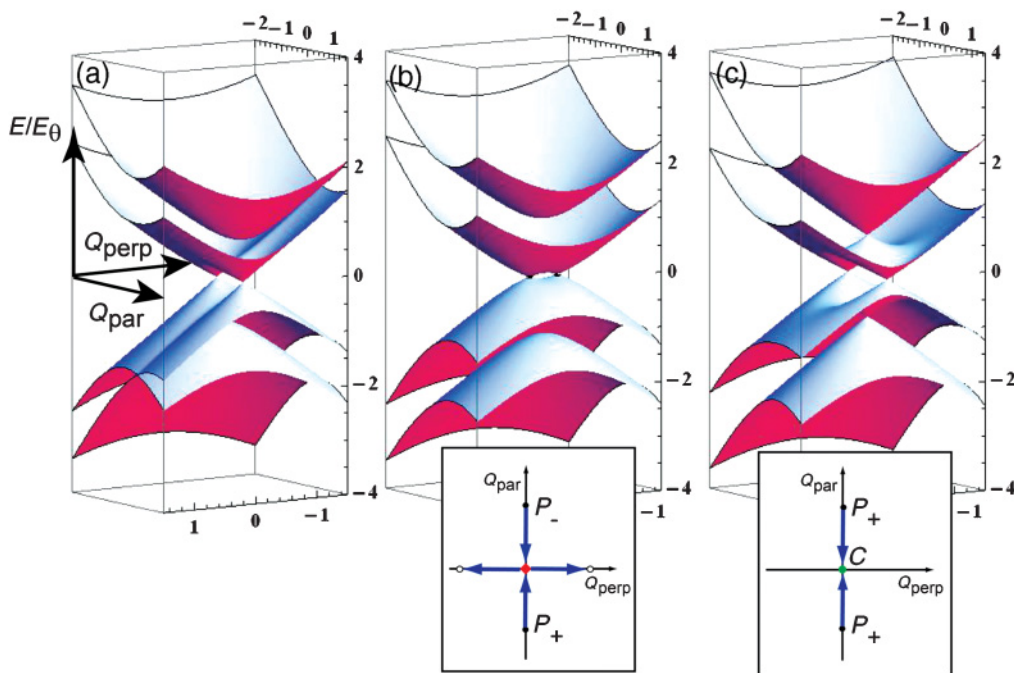


FIG. 3. (Color online) Electronic spectra for twisted bilayers using the interaction parameters (a) $\hat{t}_0 = \tilde{c}(\mathbf{I} + \sigma_x)$, $\tilde{c} = 0.21$, (b) $\hat{t}_0 = \tilde{c}\sigma_x$, $\tilde{c} = 0.55$, and (c) $\hat{t}_0 = \tilde{c}\mathbf{I}$, $\tilde{c} = 0.55$. Q_{par} and Q_{perp} are momenta in units of the offset $|\Delta\vec{K}|$ and the ordinate is the scaled energy $E/E_\theta = E/(\hbar v_F \Delta K)$. In (b), Dirac cones with opposite helicity are coupled; in (c), Dirac cones with the same helicity are coupled. The insets give the locations of singular points in the spectra describing the annihilation and regeneration of Dirac nodes (red diamond) in the compensated case (b) and the appearance of a singular point of degeneracy (C) for the uncompensated case (c). The point C is a second generation Dirac point singularity in the coupled spectrum.

earlier studies.^{8,16} The left panel of Fig. 3 shows the bilayer spectra computed in this model, which shows the expected (θ -dependent) reduction of the Dirac cone velocities and a hybridization of the two branches in the spectral region where they merge.

We now consider a refinement of the interlayer coupling matrices using the parametrization of model II. The salient properties of the SWMcC parametrization are the introduction of the interlayer amplitudes γ_3 and γ_4 with γ_3 comparable to γ_1 and γ_4 significantly smaller. Note that γ_3 and γ_4 represent interlayer hopping processes at the same range, but in different directions with respect to the layer crystallographic axes. The asymmetry between γ_3 and γ_4 thus reflects an intrinsic threefold lattice anisotropy in the interlayer amplitudes which, though symmetry-allowed, does not occur in the isotropic two-center tight-binding approximation. Significantly, these additional terms break the symmetry between the pseudospin-diagonal and off-diagonal terms in \hat{t}_0 (Table I), so that the coupling matrix is dominated by its off-diagonal amplitudes. An instructive limit considers $\hat{t}_0 \propto \sigma_x$ for which the Fig. 3(b) shows the spectrum calculated for a $\theta = 3.89^\circ$ rotation away from Bernal stacking. Here the two Dirac cones have merged at low energy, producing two composite low-energy singular points. Note that the linear low-energy dispersion is replaced by an approximately quadratic form near the center of symmetry of these spectra and that the momentum offset between the singular points in the spectrum is along the Q_{perp} axis, i.e., $\pi/2$ -rotated with respect to the original Dirac cone offset $\Delta\vec{K}$.

These spectral changes reflect the proximity to a critical point that occurs at $\tilde{c} = 1/2$ in this theory. This can be understood by considering a single-layer sublattice exchange operation implemented by the gauge transformation

$$\begin{aligned} \tilde{H} &= \begin{pmatrix} \mathbf{I} & 0 \\ 0 & \hat{\sigma}_x \end{pmatrix} \begin{pmatrix} \hat{H}_K(\vec{q}) & \tilde{c}\hat{\sigma}_x \\ \tilde{c}\hat{\sigma}_x & \hat{H}_K(\vec{q} - \Delta\vec{K}) \end{pmatrix} \begin{pmatrix} \mathbf{I} & 0 \\ 0 & \hat{\sigma}_x \end{pmatrix} \\ &= \left(\begin{array}{c|c} \hat{H}_K(\vec{q}) & \tilde{c}\mathbf{I} \\ \tilde{c}\mathbf{I} & \hat{\sigma}_x \cdot \hat{H}_K(\vec{q} - \Delta\vec{K}) \cdot \hat{\sigma}_x \end{array} \right), \end{aligned} \quad (7)$$

demonstrating that this system has a scalar coupling between Dirac cones with compensating helicities (Berry's phase $\pm\pi$). Increasing the control parameter \tilde{c} (by decreasing θ) draws the nodes together until they become coincident at a critical coupling strength $\tilde{c} = 1/2$ and annihilate [Fig. 3(b) inset]. For $\tilde{c} > 1/2$, new singularities emerge at $E = 0$ separated by $\Delta\vec{Q}$ directed perpendicular to the original offset $\Delta\vec{K}$. Using the parameters listed in Table I, $\tilde{c}(\theta = 3.89^\circ) = 0.55$, i.e., just on the strong-coupling side of this transition. The residual curvature in the low-energy spectrum and the associated reorientation of $\Delta\vec{Q}$ are both clearly evident in Fig. 3(b). It is noteworthy that the momentum separation between the zero energy contact points is not determined purely geometrically by the rotation angle, as is generally assumed, but instead is modified by the interlayer coupling. This occurs because the interactions between layers produces an effective gauge field seen within each layer that shifts the momentum of its zero-energy states. The $\pi/2$ rotation of the momentum offset

that bridges the contact points on the strong-coupling side of the transition is a striking consequence of this gauge coupling.

Reversing the sign of the threefold anisotropy in the interlayer matrix \hat{t}_0 produces a distinct electronic state. The complementary behavior is understood by considering the limit $\hat{t}_0 \propto \mathbf{I}$, which describes the coupling of Dirac cones with the same helicity, preventing annihilation of the Dirac nodes and leading to a qualitatively different geometry in the bilayer spectrum [Fig. 3(c)]. The dispersing bands from the uncoupled cones are degenerate everywhere along the line that bisects $\Delta\vec{K}$. However, along the line that connects the Dirac nodes the pseudospins of the intersecting branches are orthogonal and the interlayer coupling is symmetry-forbidden, turning on linearly as a function of the transverse momentum Q_{perp} . Thus the coupled system retains a twofold point degeneracy midway between the displaced Dirac nodes.²⁵ The cancellation of the interlayer coupling at this critical point is the bilayer analog of the “absence of backscattering” due to the π Berry’s phase in single-layer graphene. In the vicinity of this critical point, interlayer coupling is allowed and proportional to the transverse momentum. Thus this system exhibits second generation Dirac singularities in its coupled-layer spectrum as shown in Fig. 3(c): hybridization of the two layers is symmetry forbidden at a discrete critical crossing point. We refer to this complementary state as the uncompensated bilayer state.

IV. FERMI VELOCITY

The relative helicity of the two Dirac cones also controls the renormalization of their Fermi velocities, further distinguishing these two states. For Dirac cones of opposite helicities, perturbation theory on the Hamiltonian in Eq. (7) for small \tilde{c} modifies the velocity operators,

$$\begin{aligned}\hat{v}_+ &= v_F \sigma_+ \rightarrow v_F(1 - \tilde{c}^2)\sigma_+, \\ \hat{v}_- &= v_F \sigma_- \rightarrow v_F(1 - \tilde{c}^2)\sigma_-, \end{aligned} \quad (8)$$

which symmetrically reduces both v_x and v_y ; summation over the triad of offset momenta $\Delta\vec{K}_i$ yields the renormalized velocity $v_F^* = v_F(1 - 9\tilde{c}^2)$ exactly as found in earlier work.^{8,16} By contrast, for coupling between nearby cones of the same helicity, perturbation theory yields

$$\begin{aligned}\hat{v}_+ &= v_F \sigma_+ \rightarrow v_F(\sigma_+ - \tilde{c}^2\sigma_-), \\ \hat{v}_- &= v_F \sigma_- \rightarrow v_F(\sigma_- - \tilde{c}^2\sigma_+), \end{aligned} \quad (9)$$

so that in this class the corrections to the velocity are weaker, $\propto \tilde{c}^4$. Moreover, they have a twofold $\cos(2\phi)$ anisotropy, so they vanish by symmetry after summing over the threefold symmetric triad of $\Delta\vec{K}_i$. Thus the Fermi velocity is unchanged by the interlayer coupling in this class of bilayers. Physically, this can be understood by observing that the bands dispersing from the Dirac nodes are connected smoothly to the second generation points of degeneracy at $\Delta\vec{K}/2$.

V. DISCUSSION

The distinction between the compensated and uncompensated states in the small-angle limit reflects a lattice-scale property that determines the matrix structure of the long-

wavelength coupling in Eq. (1). This should be distinguished from the different mechanism by which sublattice exchange symmetry determines the direct coupling between the Dirac nodes.¹⁴ The latter requires finite momentum umklapp interlayer hopping processes which, though significant for low-order rational commensurate rotations, are negligible in the small-angle limit considered here. For example, note that sublattice exchange “even” and “odd” commensurations are related by a rigid sublattice translation of one layer at a fixed rotation angle. In the small angle regime, this translation simply permutes regions of the bilayer that are locally in AB , BA , and AA registry as shown in Fig. 1, but it does not change \hat{t}_0 , which determines the spectrum. Thus sublattice exchange even and odd structures become indistinguishable in the small-angle limit. Note also that bilayers at rotation angles θ and $\bar{\theta} = \pi/3 - \theta$ are commensuration pairs that can be distinguished by their sublattice exchange parity.¹⁴ Even- and odd-parity commensurations are, respectively, inflated generalizations of the primitive AA and AB stacked bilayers. This symmetry ultimately determines the valley structure of the interlayer amplitudes that directly couple the Dirac nodes of neighboring layers. This interlayer umklapp coupling derives from the finite momentum terms in the interlayer Hamiltonian in contrast to the $q = 0$ terms that control the physics for small-angle rotations.

The spectra for these two classes are ultimately determined by the pseudospin asymmetry in \hat{t}_0 . The conventional SWMcC model selects the class that couples cones with compensating helicities. In this model, the spectral transition illustrated in Fig. 3 occurs for rotation angles near 4° , i.e., in a range that is frequently studied experimentally.^{17,18} The physics of the uncompensated class occurs for $c_{aa} > c_{ab}$, which requires $\gamma_4 > \gamma_3$. Although this is excluded by the conventional SWMcC parametrization, it is important to note that this parametrization is designed to fit data for Bernal stacking, and it likely does not properly represent the matrix structure of the coupling in AA registered regions. In particular, using the parametrization of Table I, the spatial dependence of Eq. (1) shows that strong interlayer coupling in AA stacked regions requires $\gamma_4 > \gamma_3$. Microscopically, this originates from interlayer tunneling processes along the edges of eclipsed hexagons in the aligned AA structure, a motif which does not appear at all for Bernal stacking. In the spirit of the SWMcC theory, it is therefore appropriate to retain γ_3 and γ_4 as parameters that can be determined from the experimentally observed properties of twisted graphenes.

In fact, the phenomenology of the uncompensated class provides a striking explanation for many of the puzzling observed spectral properties for rotationally faulted graphenes thermally grown on SiC(000 $\bar{1}$).^{11,12,15} Landau-level spectroscopy shows a negligible renormalization of the Fermi velocity in these structures¹² and, furthermore, angle-resolved photoemission finds no evidence for a hybridization-induced avoided crossing of the intersecting Dirac cones, despite a careful search.¹⁵ This is completely consistent with the existence of a node in the interlayer coupling at the midpoint between offset Dirac cones characteristic of the uncompensated class. This assignment can be confirmed definitively by measurements of the quasiparticle dispersion along an azimuth passing through the midpoint between the displaced Dirac cones, but perpendicular to $\Delta\vec{K}$;

these should show a band splitting linear in the transverse momentum around the point of degeneracy. Alternatively, if these bilayers exist in the compensated class, photoemission should be able to detect the annihilation and reemergence of their singular contact points along with the band curvature in their spectra in the crossover regime as illustrated in Fig. 3(b).

By contrast, experiments on rotationally faulted chemical vapor deposition (CVD)-grown graphenes have observed phenomena that have been associated with the spectral properties of the compensated class.^{18,20} Features due to the van Hove singularities arising from the avoided crossing of hybridized Dirac cones¹⁸ and a θ -dependent low-energy velocity renormalization have both been reported.²⁰ These features are at least qualitatively consistent with the predicted behavior of the compensated class and have been analyzed within a theoretical model representative of this class.⁸ We note that these measurements study samples at small rotation angle, where the proximity to the merger of the Dirac singularities (Fig. 3) should be manifest in these data, though their effects have not yet been considered in the analysis. It is interesting that these samples exhibit a large periodic height modulation $\approx 1 \text{ \AA}$ in the superlattice unit cell peaked in the AA -registered zones.²⁶ It is tempting to speculate that these CVD samples are grown as rippled structures that partially delaminate in these regions, thereby locally weakening their contribution to the $q = 0$ coupling coefficients. In this scenario, the strongly coupled regions would maintain Bernal registry as described by the conventional SWMcC parametrization and

identify these samples as members of the compensated bilayer family.

The distinction between the two complementary states is controlled by an important threefold anisotropy in the interlayer tunneling amplitudes. This physics is not captured by an isotropic two-center tight-binding theory, which inevitably leads one to the coupling model in Eq. (6), which happens to occur at a crossover between two rather different electronic models for the system. The effects of the threefold anisotropy are accessible in density-functional calculations of these structures, but for practical reasons these have been restricted to short period superlattices that do not address the small-angle regime where the continuum theory is most appropriate. For short-period commensurate structures, the Fermi velocities found in these calculations are consistent with the values for single-layer graphene. This could arise from the small value of \tilde{c} in the large-angle regime, the intrinsic behavior of the uncompensated class, or an interlayer mass term, which is important for short period superlattices.¹⁴

ACKNOWLEDGMENTS

I thank P. First, C. Kane, M. Kindermann, S. Zaheer, and F. Zhang for their comments on the manuscript and E. Andrei for communication of unpublished data. This work was supported by the Department of Energy, Office of Basic Energy Sciences under Contract No. DE-FG02-ER45118.

*mele@physics.upenn.edu

¹E. McCann and V. I. Fal'ko, *Phys. Rev. Lett.* **96**, 086805 (2006).

²T. Ohta *et al.*, *Science* **313**, 951 (2006).

³F. Guinea, A. H. Castro Neto, and N. M. R. Peres, *Phys. Rev. B* **73**, 245426 (2006).

⁴H. Min and A. H. MacDonald, *Phys. Rev. B* **77**, 155416 (2008).

⁵M. Koshino and E. McCann, *Phys. Rev. B* **80**, 165409 (2009).

⁶C. Berger *et al.*, *Science* **312**, 1191 (2006).

⁷S. Latil, V. Meunier, and L. Henrard, *Phys. Rev. B* **76**, 201402(R) (2007).

⁸J. M. B. Lopes dos Santos, N. M. R. Peres, and A. H. Castro Neto, *Phys. Rev. Lett.* **99**, 256802 (2007).

⁹J. Hass, F. Varchon, J. E. Millán-Otoya, M. Sprinkle, N. Sharma, W. A. de Heer, C. Berger, P. N. First, L. Magaud, and E. H. Conrad, *Phys. Rev. Lett.* **100**, 125504 (2008).

¹⁰S. Shallcross, S. Sharma, and O. A. Pankratov, *Phys. Rev. Lett.* **101**, 056803 (2008).

¹¹M. Sprinkle, D. Siegel, Y. Hu, J. Hicks, A. Tejada, A. Taleb-Ibrahimi, P. Le Fèvre, F. Bertran, S. Vizzini, H. Enriquez, S. Chiang, P. Soukiassian, C. Berger, W. A. de Heer, A. Lanzara, and E. H. Conrad, *Phys. Rev. Lett.* **103**, 226803 (2009).

¹²D. M. Miller, K. D. Kubista, G. M. Rutter, W. A. de Heer, P. N. First, and J. A. Stroscio, *Science* **324**, 9242 (2009).

¹³G. T. Laissardiere, D. Mayou, and L. Magaud, *Nano Lett.* **10**, 804 (2010).

¹⁴E. J. Mele, *Phys. Rev. B* **81**, 161405 (2010).

¹⁵J. Hicks, M. Sprinkle, K. Shepperd, F. Wang, A. Tejada, A. Taleb-Ibrahimi, F. Bertran, P. Le Fèvre, W. A. de Heer, C. Berger, and E. H. Conrad, *Phys. Rev. B* **83**, 205403 (2011).

¹⁶R. Bistritzer and A. H. MacDonald, *Proc. Natl. Acad. Sci. USA* **108**, 12233 (2011).

¹⁷G. Li, A. Luican, and E. Y. Andrei, *Phys. Rev. Lett.* **102**, 176804 (2009).

¹⁸G. Li, A. Luican, J. M. B. Lopes dos Santos, A. H. Castro Neto, A. Reina, J. Kong, and E. Y. Andrei, *Nature Phys.* **6**, 109 (2010).

¹⁹M. Kindermann and P. N. First, *Phys. Rev. B* **83**, 045425 (2011).

²⁰A. Luican, G. Li, A. Reina, J. Kong, R. R. Nair, K. S. Novoselov, A. K. Geim, and E. Y. Andrei, *Phys. Rev. Lett.* **106**, 126802 (2011).

²¹R. de Gail, M. O. Goerbig, F. Guinea, G. Montambaux, and A. H. Castro Neto, *Phys. Rev. B* **84**, 045436 (2011).

²²M.-Y. Choi, Y.-H. Hyun, and Y. Kim, *Phys. Rev. B* **84**, 195437 (2011).

²³M. Freitag, *Nature Phys.* **7**, 596 (2011).

²⁴M. S. Dresselhaus and G. Dresselhaus, *Adv. Phys.* **51**, 69 (2002).

²⁵Because of the rotation of σ_θ in Eq. (6), this point degeneracy is slightly shifted along the line that bisects $\Delta\vec{K}$. This does not significantly change the physics.

²⁶E. Y. Andrei (unpublished).